

# Observation of Dipolar Spin-ice-like Correlations in the Quantum Spin Ice Candidate $\text{Ce}_2\text{Sn}_2\text{O}_7$

B. Yuan,<sup>1</sup> M. Powell,<sup>2</sup> X. Liu,<sup>1</sup> J. Ni,<sup>1</sup> E. M. Smith,<sup>1</sup> F. Ye,<sup>3</sup>  
 J. Dudemaine,<sup>4,5</sup> A. D. Bianchi,<sup>4,5,6</sup> J. W. Kolis,<sup>2</sup> and B. D. Gaulin<sup>1,7,8</sup>

<sup>1</sup>*Department of Physics and Astronomy, McMaster University, Hamilton, Ontario L8S 4M1, Canada*

<sup>2</sup>*Department of Chemistry, Clemson University, Clemson, South Carolina 29634-0973, USA*

<sup>3</sup>*Neutron Scattering Division, Oak Ridge National Laboratory, Oak Ridge, Tennessee 37831, USA*

<sup>4</sup>*Département de Physique, Université de Montréal, Montréal, Québec, Canada*

<sup>5</sup>*Regroupement Québécois sur les Matériaux de Pointe (RQMP)*

<sup>6</sup>*Institut Courtois, Complexe des sciences, Université de Montréal,*

*1375 Ave. Thérèse-Lavoie-Roux, Montréal, Québec H2V 0B3, Canada*

<sup>7</sup>*Brockhouse Institute for Materials Research, McMaster University, Hamilton, Ontario L8S 4M1, Canada*

<sup>8</sup>*Canadian Institute for Advanced Research, 661 University Avenue, Toronto, Ontario M5G 1M1, Canada.*

(Dated: January 29, 2026)

The  $\text{Ce}_2\text{X}_2\text{O}_7$  ( $\text{X}=\text{Sn}, \text{Hf}, \text{Zr}$ ) family of cubic pyrochlores has emerged as one of the most promising classes of Quantum Spin Ice candidates. However, understanding their microscopic exchange Hamiltonian and spin correlations has been hampered by varying sample quality, and poor signal-to-noise in the existing neutron data due to a small  $\text{Ce}^{3+}$  magnetic dipole moment. In this work, we overcome these challenges and report single-crystal diffuse neutron scattering from hydrothermally grown  $\text{Ce}_2\text{Sn}_2\text{O}_7$  – the highest quality crystals obtained to date for the  $\text{Ce}_2\text{X}_2\text{O}_7$  family. In contrast to the broad diffuse scattering observed in  $\text{Ce}_2\text{Hf}_2\text{O}_7$  and  $\text{Ce}_2\text{Zr}_2\text{O}_7$ , we find highly structured diffuse scattering from  $\text{Ce}_2\text{Sn}_2\text{O}_7$  featuring strong intensities along the Brillouin zone boundaries. The observed  $\mathbf{Q}$ -dependence disagrees with predictions of the nearest neighbour XYZ model commonly used for  $\text{Ce}_2\text{X}_2\text{O}_7$ , but is remarkably similar to the diffuse scattering observed in *classical* Dipolar Spin Ice. Our study highlights the importance of further neighbour interactions in determining the low energy physics of the Ce-pyrochlores, and calls for a revision of the current theoretical framework to incorporate their effects.

*Introduction*—Rare-earth (RE) pyrochlores, featuring a corner-sharing network of RE-ion tetrahedra, have been a cornerstone in quantum magnetism research. At the heart of these materials is the presence of a highly degenerate low-energy manifold of 2-in-2-out (2I2O) spin configurations when the RE moments are coupled by a ferromagnetic Ising-like interaction. Although the 2I2O manifold, with its highly nontrivial topological properties [1], is interesting in its own right, its real appeal, and the main impetus for spin-ice research, lies in the rich spectrum of exotic phases that emerges when its degeneracy is lifted by interactions beyond the nearest neighbour (NN) Ising model. The ‘Coulomb phase’ found in classical Dipolar Spin Ice (DSI) materials such as  $\text{Dy}_2\text{Ti}_2\text{O}_7$  [2, 3] and  $\text{Ho}_2\text{Ti}_2\text{O}_7$  [4, 5] is the earliest, and perhaps the most famous example of this. In DSIs, the degeneracy of the 2I2O manifold is lifted by long-range magnetic dipolar and further neighbour exchange interactions [6, 7]. The significant modifications of the low energy landscape and spin correlations accompanying this degeneracy breaking are directly manifested in a neutron scattering experiment as a transfer of the diffuse scattering intensity from the well-known snow-flake pattern with sharp pinch points to Brillouin zone boundaries [2, 5].

More recently, much spin-ice research has focused on the search for ‘Quantum Spin Ice’ (QSI) – a quantum spin liquid phase that emerges from the coherent superposition of all or a subset of the 2I2O manifold [8, 9]. Despite its potential to host many exotic excitations

such as the emergent ‘photons’ [8, 10], the experimental realization of QSI in actual RE-pyrochlores has remained elusive because of the stringent criteria on the exchange Hamiltonian. On the one hand, sizeable transverse exchange terms must be present to enable quantum fluctuations and tunneling between different 2I2O state. On the other, these interactions cannot be too large, or out-weighed by other competing interactions, inevitably present in real materials, that pull the system into other competing phases. In addition to the long-range interactions in the DSIs, other examples include bond-dependent anisotropic NN exchange in  $\text{Yb}^{3+}$ -based [11–14] and  $\text{Er}^{3+}$ -based [15–17] pyrochlores with a Kramers’ doublet single-ion ground state (GS), and defect-induced effective random transverse fields in  $\text{Pr}^{3+}$ -pyrochlores with a non-Kramers’ doublet GS [18–22]. These effects have pre-empted QSI states in these earlier candidates, where they gave rise to exotic but ordered [16], and spin-frozen states [19, 20, 22], respectively.

These caveats for previous QSI candidates seem to be overcome in the recently discovered dipole-octupole (DO)-pyrochlores based on  $\text{Nd}^{3+}$  and  $\text{Ce}^{3+}$ . The unique symmetry property of their Kramers’ doublet GS wavefunctions defines an unusual pseudospin- $\frac{1}{2}$  degree of freedom whose  $S_x/S_z$  and  $S_y$ -components transform differently under point group and time reversal symmetry, as dipoles and octupoles, respectively [23, 24]. These unique properties constrain the NN interaction to take a remarkably simple XYZ form,  $J_{\tilde{x}}S_{\tilde{x},i}S_{\tilde{x},j} + J_{\tilde{y}}S_{\tilde{y},i}S_{\tilde{y},j} +$

$J_{\tilde{z}}S_{\tilde{z},i}S_{\tilde{z},j}$ , after a rotation about the local  $\hat{y}$ -axis by a material-dependent angle,  $\theta$ , such that  $S_z = S_{\tilde{z}} \cos \theta + S_{\tilde{x}} \sin \theta$  [23, 24]. In the absence of further neighbour coupling, the phase diagram of this XYZ model has been well established to support a QSI state with a dominant  $J_{\tilde{\alpha}} > 0$ , which, depending on whether  $J_{\tilde{x}/\tilde{z}}$  or  $J_{\tilde{y}}$  dominates, is either dipolar (D-QSI) or octupolar (O-QSI) in nature [25, 26]. The validity of the simple XYZ model with a dominant  $J_{\tilde{x}} > 0$  has been firmly established in  $\text{Nd}_2\text{X}_2\text{O}_7$  (X=Sn, Hf, Zr) through fitting the magnon spectrum in the ordered phase to linear spin wave theory[27–30]. This places them in close proximity to a D-QSI state, although a sizeable, unfrustrated  $J_{\tilde{z}} < 0$  eventually gives rise to an all-in-all-out (AIAO) order at low temperatures in  $\text{Nd}_2\text{X}_2\text{O}_7$ .

The other class of DO-pyrochlores, namely  $\text{Ce}_2\text{X}_2\text{O}_7$  (X=Sn, Hf, Zr), has captured most recent attention, [31–44], with promising discoveries of a broad spin-ice-like diffuse scattering pattern and an inelastic scattering continuum in all of them. However, in contrast to  $\text{Nd}_2\text{X}_2\text{O}_7$ , whose exchange parameters have been very well established, less is known about the detailed microscopic Hamiltonian and spin correlations in these Ce-pyrochlores for two reasons. First is the issue of sample quality arising from  $\text{Ce}^{3+}$ 's tendency to oxidize to the more stable non-magnetic  $\text{Ce}^{4+}$  [32, 40]. This issue has been addressed in  $\text{Ce}_2\text{Sn}_2\text{O}_7$  by the recent advances in hydrothermal growth of  $\text{RE}_2\text{Sn}_2\text{O}_7$  that substantially reduces the synthesis temperature from over  $2000^\circ \text{C}/1000^\circ \text{C}$  used in conventional floating zone/solid-state growth to  $700^\circ \text{C}$  [14]. The importance of using a high quality sample has been highlighted by the contradictory neutron powder diffraction (NPD) results on *powder* samples grown by different methods: a broad high- $|\mathbf{Q}|$  scattering attributed to octupolar scattering was observed in earlier samples grown using the solid-state methods [34], while only low- $|\mathbf{Q}|$  scattering consistent with a proximate D-QSI is observed in the better quality, hydrothermally grown samples [38]. Second and perhaps more fundamentally, instead of relying on a variety of experimental techniques (i.e. both bulk and neutron scattering measurements), the microscopics in  $\text{Ce}_2\text{X}_2\text{O}_7$  have been largely determined by modeling high-temperature bulk measurements, *assuming* the validity of an XYZ model [35, 38, 40, 45]. Existing neutron scattering data on  $\text{Ce}_2\text{X}_2\text{O}_7$  suffer from relatively poor signal-to-noise ratio, owing in part to the small  $\text{Ce}^{3+}$  moment and, in the case of  $\text{Ce}_2\text{Sn}_2\text{O}_7$ , to the lack of high-quality large single crystals, and have been less useful in constraining the detailed spin correlations or exchange parameters in these systems.

To address these challenges, we carried out the first *single-crystal* diffuse scattering measurement on a co-aligned array of hydrothermally grown single crystals of  $\text{Ce}_2\text{Sn}_2\text{O}_7$ , with a significantly lower level of defect than our previous floating zone grown  $\text{Ce}_2\text{Zr}_2\text{O}_7$  (See Supplemental Materials for details of sample characterization and experimental methods). These measurements used

the CORELLI spectrometer [46] at the Spallation Neutron Source (SNS). In agreement with the previous NPD results [38], we only observed the low- $|\mathbf{Q}|$  'dipolar' scattering. The high crystal quality, together with a dramatic improvement in signal-to-noise ratio enabled by the large reciprocal space coverage at CORELLI (see *Results*), and the increased power of its SNS source, uncovered a  $\mathbf{Q}$ -dependence of the diffuse scattering intensity that defies the predictions of the nearest neighbour XYZ model proposed previously [38]. The observed diffuse scattering pattern, featuring strong intensities along the Brillouin zone boundaries, is almost identical to that observed in DSIs [2] and provides compelling evidence for the importance of further neighbour interactions beyond the NN model.

*Results*– Energy-integrated neutron intensity maps at 50 mK in the HHL [Fig. 1(a)] and HK0 plane [Fig. 1(b)] (a 12 K background has been subtracted from all data in Fig. 1) reveal a highly structured 3-dimensional diffuse scattering pattern in  $\text{Ce}_2\text{Sn}_2\text{O}_7$ . The pattern essentially disappears at 800 mK [Fig. 1(c, d)], confirming its magnetic origin. Our data clearly show that the diffuse scattering in  $\text{Ce}_2\text{Sn}_2\text{O}_7$  is concentrated along the Brillouin zone (BZ) boundaries of the underlying FCC lattice (indicated by white solid lines in Fig. 1). The intensity is maximized in the first BZ and weakens at larger  $|\mathbf{Q}|$ , consistent with the expected behaviour of the dipolar form factor [41]. The data presented in Fig. 1 is of markedly better quality than previous measurements on  $\text{Ce}_2\text{Zr}_2\text{O}_7$  [32, 33] and  $\text{Ce}_2\text{Hf}_2\text{O}_7$  [40], which observed a ring-like diffuse signal along the boundary of the first BZ qualitatively similar to the present data, but only a broad  $\mathbf{Q}$ -dependence beyond the first zone. In contrast, the diffuse scattering in  $\text{Ce}_2\text{Sn}_2\text{O}_7$  remains well-defined and unambiguously resides along the FCC BZ boundaries even in the second and third BZs [e.g. around (222) in Fig. 1(a)]. In addition to a dramatic improvement in crystal quality, a key to the exceptional data quality in Fig. 1 is the large reciprocal space coverage at CORELLI (enabled by the use of thermal neutrons and a large detector coverage in the horizontal and vertical directions), that probes *all* symmetry equivalent directions in the full *3-dimensional* reciprocal space. Folding the data by *all* symmetry operations of the cubic space group significantly improves the signal-to-noise ratio (See Supplemental Materials).

The large reciprocal space coverage also enabled us to study the magnetic correlations in  $\text{Ce}_2\text{Sn}_2\text{O}_7$  at large  $|\mathbf{Q}|$ 's. Following our previous analysis of the  $\text{Ce}_2\text{Zr}_2\text{O}_7$  CORELLI data [41], we examined the diffuse scattering in the  $[\text{H}+0.5, \text{H}-0.5, \text{L}]$  plane (inset of Fig. 2) which contains no nuclear Bragg peaks (powder rings due to the sample environment and the sample holder have also been removed). Other than the zone boundary (ZB) scattering at low  $|\mathbf{Q}|$ 's, our data shows no obvious magnetic scattering beyond  $|\mathbf{Q}| \sim 3 \text{\AA}^{-1}$  (or  $\text{L} \sim 5$ ). To directly compare with the previous NPD measurements, we performed an orientational average of the single crystal data in Fig. 2 to obtain the diffuse scattering intensity as a

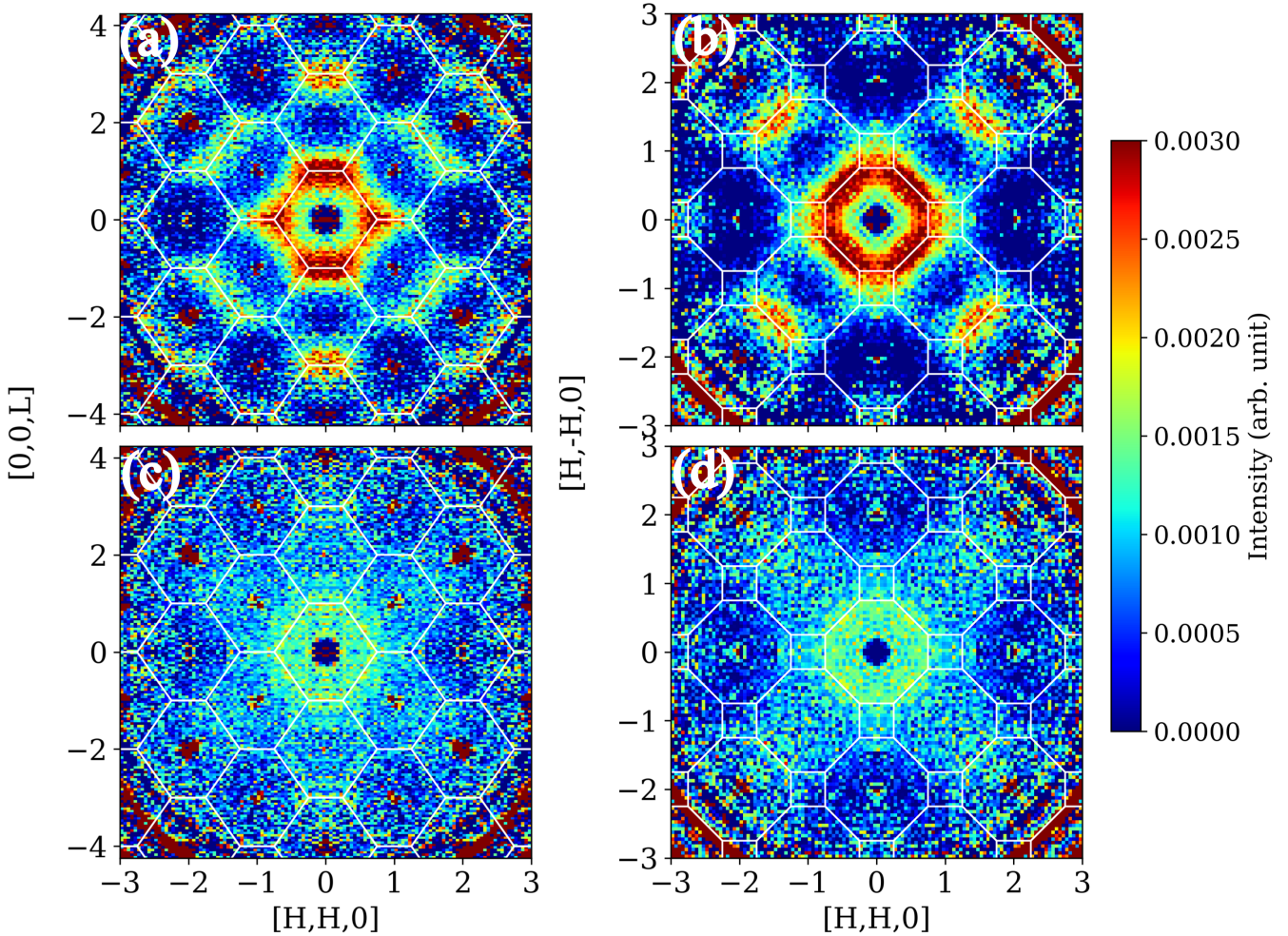


FIG. 1.  $\text{Ce}_2\text{Sn}_2\text{O}_7$  diffuse neutron scattering in the (a,c) HHL and (b,d) HK0 plane at (a,b) 50 mK and (c,d) 800 mK. A 12 K background has been subtracted from all the data. The data in (a,c)/(b,d) is obtained by integrating the diffuse intensity in the  $[\text{H}, \text{H}, 0]/[0, 0, \text{L}]$  direction with  $-0.2 < \text{H} < 0.2/-0.2 < \text{L} < 0.2$ , and has been symmetrized in accordance with the  $Fd\bar{3}m$  space group. The white lines denote the Brillouin zone boundaries of the primitive FCC lattice.

function of  $|\mathbf{Q}|$ . The resulting powder-averaged spectrum (main panel of Fig. 2), featuring a strong peak at  $|\mathbf{Q}| \sim 0.6 \text{ \AA}^{-1}$  and a temperature-independent flat background at  $|\mathbf{Q}| \gtrsim 3 \text{ \AA}^{-1}$ , is in excellent agreement with the previous NPD results on hydrothermally grown  $\text{Ce}_2\text{Sn}_2\text{O}_7$  powder [38]. This is to be contrasted with NPD on powder samples grown by conventional solid state method showing a broad peak centered at  $|\mathbf{Q}| \sim 8 \text{ \AA}^{-1}$  that was attributed to octupolar scattering [34]. The failure to observe any octupolar scattering in  $\text{Ce}_2\text{Sn}_2\text{O}_7$ , and previously in  $\text{Ce}_2\text{Zr}_2\text{O}_7$ , has been argued to be a simple consequence of the much larger dipolar form factor in these DO compounds [41], which gives rise to a dominant low  $|\mathbf{Q}|$  dipolar scattering even in systems with dominant octupolar interactions (e.g.  $\text{Ce}_2\text{Zr}_2\text{O}_7$ ).

*Discussions-* The observed diffuse scattering in Fig. 1(a) [reproduced in Fig. 3(a)] reveals a departure of the low energy physics in  $\text{Ce}_2\text{Sn}_2\text{O}_7$  from the predictions by the nearest neighbour XYZ model proposed

in Ref. [38]. This is clear by comparing Fig. 3(a) to the diffuse scattering in  $\text{Nd}_2\text{Zr}_2\text{O}_7$  [Fig. 3(c)], which is ascribed an exchange Hamiltonian similar to that proposed for  $\text{Ce}_2\text{Sn}_2\text{O}_7$ . Unlike  $\text{Ce}_2\text{Sn}_2\text{O}_7$ , whose exchange parameters (within the XYZ model) were only established through modeling of bulk measurements to be  $\{J_{\bar{x}} > 0, J_{\bar{y}} \approx 0, J_{\bar{z}} \approx -0.3J_{\bar{x}}, \theta \approx 0.2\pi\}$  [38], the pseudospin Hamiltonian in  $\text{Nd}_2\text{Zr}_2\text{O}_7$  has been determined to be  $\{J_{\bar{x}} > 0, J_{\bar{y}} \approx 0, J_{\bar{z}} \approx -0.5J_{\bar{x}}, \theta \approx 0.3\pi\}$  by both bulk measurements and linear spin-wave fitting of the magnon spectrum below  $T_N$  [27–29]. Both sets of parameters predict a weak AIAO order in the  $S_{\bar{z}}$ -sector with a suppressed  $T_N$ , proximate to a D-QSI phase in the  $S_{\bar{x}}$ -sector [38]. The phase right above  $T_N$  therefore features competing spin-ice- and AIAO-like correlations. Coexistence of the two types of spin correlations is entirely consistent with the diffuse scattering computed by numerical linked cluster (NLC) [48] and classical Monte Carlo [47] methods, predicting broad peaks at the AIAO

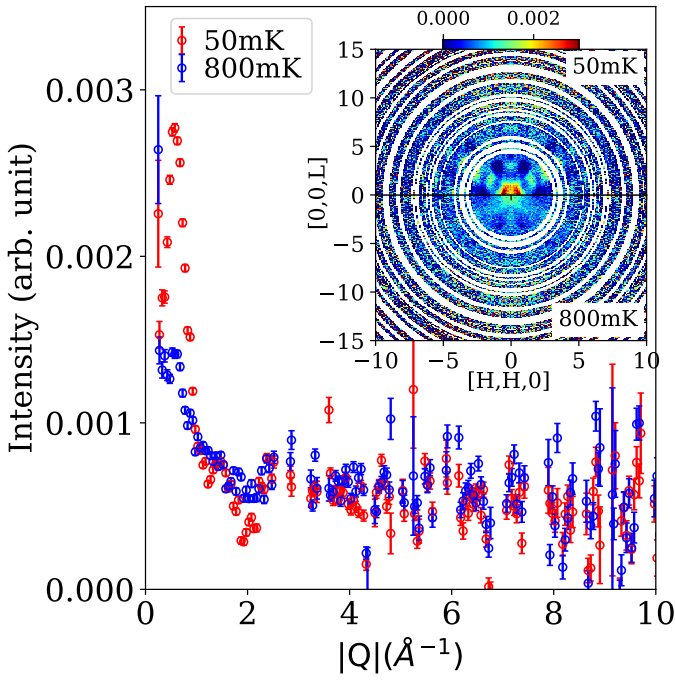


FIG. 2. Powder-averaged diffuse scattering intensity as a function of  $|Q|$  at 50 mK and 800 mK obtained by performing an orientational average of the symmetrized single crystal data in the  $[H+0.5, H-0.5, L]$  plane (inset). To avoid the  $\text{Ce}_2\text{Sn}_2\text{O}_7$  nuclear Bragg peaks, we used an integration range of  $0.3 < H < 0.7$  in the  $[H, -H, 0]$  direction. A 12 K background has been subtracted from both the single crystal and powder-averaged data. Powder rings due to aluminum sample can of the dilution insert and the copper sample mount have also been masked out in the data.

ordering wave-vectors [e.g. (220) and (113)] on top of a snow-flake pattern. Such a scenario is clearly observed in  $\text{Nd}_2\text{Zr}_2\text{O}_7$  right above a  $T_N \approx 400$  mK [Fig. 3(c)] but inconsistent with Fig. 3(a) for  $\text{Ce}_2\text{Sn}_2\text{O}_7$ . First, neither magnetic Bragg peaks (see Supplemental Materials) nor broad peaks consistent with AIAO order/correlations are observed at the experimental temperature of  $\sim 50$  mK, close to the predicted  $T_N \sim 50$  mK [38]. Moreover, instead of rod-like scattering connecting pinch points as expected for a quasi-degenerate 2I2O manifold [e.g. see the broad intensities joining (111) and (222), (002) and (004) in Fig. 3(c)], the diffuse neutron scattering is concentrated near the ZBs in  $\text{Ce}_2\text{Sn}_2\text{O}_7$ .

Instead of a proximate QSI, the observed ZB scattering much more closely resembles the classical DSI  $\text{Dy}_2\text{Ti}_2\text{O}_7$  [Fig. 3(d) [6]]. In addition to observing strong intensities near (001), (003) and  $(\frac{3}{2}, \frac{3}{2}, \frac{3}{2})$ , with  $I_{(100)} > I_{(003)} > I_{(\frac{3}{2}, \frac{3}{2}, \frac{3}{2})}$  like  $\text{Dy}_2\text{Ti}_2\text{O}_7$ , the excellent data quality in Fig. 3 (a) enabled us to resolve very weak intensities along the ZB's through  $(0.5, 0.5, 2.5)$  and  $(1.5, 1.5, 2.5)$ . Remarkably, as shown in Fig. 3(e,f), representative cuts along  $[0, 0, L]$  (e) and  $[H, H, 2.375]$  (f) through the ZBs reveal almost identical  $\mathbf{Q}$ -dependence of the diffuse scattering (both the line-shape and relative intensities) in

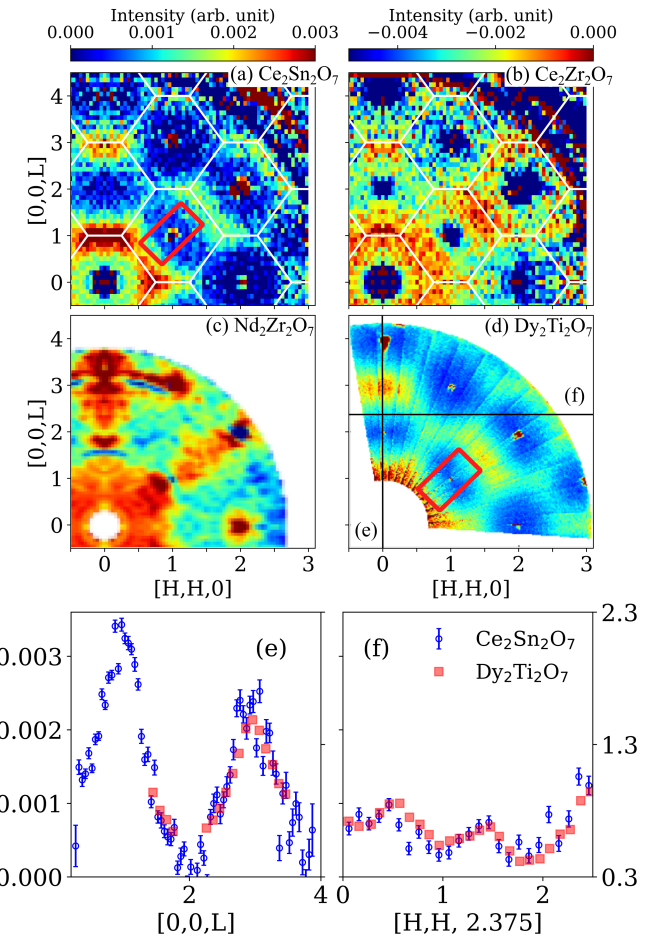


FIG. 3. (a-d) Diffuse scattering in the  $[H, H, L]$  plane in (a)  $\text{Ce}_2\text{Sn}_2\text{O}_7$  at 50mK, (b)  $\text{Ce}_2\text{Zr}_2\text{O}_7$  at 50mK, (c)  $\text{Nd}_2\text{Zr}_2\text{O}_7$  at 450mK and (d)  $\text{Dy}_2\text{Ti}_2\text{O}_7$  at 300mK. A high temperature background at 12 K/5 K/20 K has been subtracted from (a)/(b)/(c), but not (d). (a) is the same as Fig. 1 (a). (b) is part of the CORELLI data set previously published in Ref. [41]. (c) and (d) are adapted from Ref. [47] and Ref. [6], with permissions from the American Physical Society. (e,f) Diffuse scattering intensity as a function of momentum transfer along (e)  $[0, 0, L]$  and (f)  $[H, H, 2.375]$  in  $\text{Ce}_2\text{Sn}_2\text{O}_7$  (blue open circle) and  $\text{Dy}_2\text{Ti}_2\text{O}_7$  (red solid square), with intensity scales shown on the left and right vertical axes, respectively. The directions of the momentum transfers are shown as black solid lines in (d). The  $\text{Ce}_2\text{Sn}_2\text{O}_7$  data in (e) and (f) are obtained by slicing the single crystal data in (a) with an integration range of  $-0.2 < H < 0.2$  along  $[H, H, 0]$  and  $2.2 < L < 2.55$  along  $[0, 0, L]$ , respectively. The  $\text{Dy}_2\text{Ti}_2\text{O}_7$  data have been adapted from Ref. [2] with permissions from the American Physical Society.

$\text{Ce}_2\text{Sn}_2\text{O}_7$  and  $\text{Dy}_2\text{Ti}_2\text{O}_7$ . The strong resemblance of the diffuse scattering pattern, and hence the spin correlations, in  $\text{Ce}_2\text{Sn}_2\text{O}_7$  and  $\text{Dy}_2\text{Ti}_2\text{O}_7$ , provide compelling evidence for similar low energy landscapes in both compounds. Extensive earlier studies of DSI [6, 7], highlighted the dominant role played by the long-range interactions in lifting the degeneracy of the 2I2O manifold. In

particular, the failure to observe any signatures for the AIAO order near the nominal  $T_N$  predicted by the XYZ model suggests that these interactions could completely counter the effects of a sizeable  $J_z \approx -0.3J_{\tilde{x}}$  [38], and may therefore be highly non-perturbative in  $\text{Ce}_2\text{Sn}_2\text{O}_7$  – a scenario not considered in the analysis of bulk measurements [38].

At this stage, it might be tempting to apply the same theoretical framework previously used for DSI, the so-called ‘generalized dipolar spin ice model’ or g-DSI featuring both magnetic dipolar and further neighbour exchange interactions, to  $\text{Ce}_2\text{Sn}_2\text{O}_7$  [6, 7]. However, we caution against such a naive application because of the fundamentally different natures of pseudo-spins in these systems. In addition to an almost two-orders-of-magnitude reduction of magnetic dipolar interaction ( $\propto m^2$  with  $m_{\text{Ce}^{3+}} \approx 1.2 \mu_B \ll m_{\text{Dy}^{3+}} \approx 10 \mu_B$ ), the coupling between DO doublets in Ce-pyrochlores can have sizeable transverse components (all of  $J_{\tilde{\alpha}}$ ,  $\alpha = \tilde{x}, \tilde{y}, \tilde{z}$  can be non-zero) in contrast to an Ising-like interaction between the  $|\pm \frac{15}{2}\rangle$  doublet in  $\text{Dy}_2\text{Ti}_2\text{O}_7$  [49]. Finite tunneling within and out of the 2I2O manifold, suppressed in Ising-like DSI, gives rise to non-trivial QSI dynamics observed in Ce-pyrochlores [42, 43], and might explain the apparent absence of the bow-tie-shaped scattering near the pinch points in  $\text{Ce}_2\text{Sn}_2\text{O}_7$  [highlighted by red rectangle in Fig. 3(a, c)].

Incidentally, we note an interesting similarity between the  $\mathbf{Q}$ -dependence of the diffuse scattering in  $\text{Ce}_2\text{Sn}_2\text{O}_7$ , and that of the predicted QSI photon structure factor [10]– both featuring strong ZB scattering and suppressed intensity near the pinch points. Future diffuse scattering using polarized neutrons (which isolated the weak bow-tie-shaped scattering from the dominant ZB scattering, and confirmed the presence of ice-rules in DSIs [4]) as well as single crystal inelastic neutron scattering are desirable to provide a microscopic explanation for this unusual  $\mathbf{Q}$ -dependence and its uncanny similarity to DSIs despite potentially very different exchange Hamiltonians in these systems.

Beyond  $\text{Ce}_2\text{Sn}_2\text{O}_7$ , we have revisited our earlier CORELLI data on  $\text{Ce}_2\text{Zr}_2\text{O}_7$ , the high  $|\mathbf{Q}|$ -portion of which was previously published in Ref. [41]. In addition to the previously observed scattering around the first BZ [33, 40], the diffuse scattering in  $\text{Ce}_2\text{Zr}_2\text{O}_7$  in Fig. 3(b) also shows significant ZB scattering at larger  $|\mathbf{Q}|$ ’s qualitatively similar to  $\text{Ce}_2\text{Sn}_2\text{O}_7$  [Fig. 3(a)], suggesting the importance of further neighbour interactions in  $\text{Ce}_2\text{Zr}_2\text{O}_7$ . However, we note potentially very different microscopic explanations for the ZB scattering in  $\text{Ce}_2\text{Sn}_2\text{O}_7$  and  $\text{Ce}_2\text{Zr}_2\text{O}_7$ . Unlike  $\text{Ce}_2\text{Sn}_2\text{O}_7$  with a dominant *dipolar* interaction,  $J_{\tilde{x}}$ , and a sizeable  $\theta$  [38],

$\text{Ce}_2\text{Zr}_2\text{O}_7$  has a large *octupolar* interaction,  $J_{\tilde{y}} \gtrsim J_{\tilde{x}}$ , but negligible  $J_{\tilde{z}}$  and  $\theta$  [35, 45]. The diffuse scattering in  $\text{Ce}_2\text{Zr}_2\text{O}_7$  [Fig. 3 (b)] (which probes  $S_z \approx S_{\tilde{z}}$  with  $\theta \approx 0$ ) therefore solely arises from the ice-rule–*violating* transverse pseudo-spin fluctuations, whereas that in  $\text{Ce}_2\text{Sn}_2\text{O}_7$  is a sum of both longitudinal and transverse fluctuations – a consequence of finite  $\theta$  and a dominant  $J_{\tilde{x}}$ . As shown by Ref. [45], the transverse fluctuations in  $\text{Ce}_2\text{Zr}_2\text{O}_7$  are highly sensitive to further neighbour interactions, and a small next nearest neighbour interaction is sufficient to transfer the spectral weight from the rod-like scattering to the ZBs, although a full modeling of the diffuse scattering in Fig. 3 (b) likely requires the consideration of structural defects in  $\text{Ce}_2\text{Zr}_2\text{O}_7$ , that are much reduced or absent in  $\text{Ce}_2\text{Sn}_2\text{O}_7$  (see Supplemental Materials).

*Conclusions*– In summary, by carrying out diffuse neutron scattering measurements on hydrothermally grown  $\text{Ce}_2\text{Sn}_2\text{O}_7$  single crystals – the highest quality single crystals so far from the  $\text{Ce}_2\text{X}_2\text{O}_7$  family, we observed strong ZB scattering, almost identical to that observed previously in the DSI  $\text{Dy}_2\text{Ti}_2\text{O}_7$ . We also failed to detect any signatures – magnetic Bragg peaks or short-range correlations, for the AIAO order predicted by the nearest neighbour XYZ model down to the lowest experimentally accessible temperature of  $\sim 50$  mK, close to the predicted  $T_N$ . Our results provide compelling *microscopic* evidence for a determining role played by the long-range exchange and/or dipolar interactions in shaping the low energy physics in  $\text{Ce}_2\text{Sn}_2\text{O}_7$ . Notably, our bulk specific heat measurements on  $\text{Ce}_2\text{Zr}_2\text{O}_7$  [35] and  $\text{Ce}_2\text{Hf}_2\text{O}_7$  [40] also observed a clear deviation from the XYZ model for an extended low temperature range, but still *above* the lower cutoff for the numerical methods used [40], which, in conjunction with the present work, call for a critical re-assessment of the exchange Hamiltonian for the Ce-pyrochlores.

## ACKNOWLEDGEMENT

We acknowledge illuminating discussions with F. Desrochers, M.J.P. Gingras, Y.B. Kim, J.G. Rau, R. Schaefer, O. Benton, B. Placke, R. Moessner and Z. Shou. This work was supported in part by NSERC of Canada. The synthesis and crystal growth of the samples was performed at Clemson University supported by DOE grant DE-SC0020071. A portion of this research used resources at the Spallation Neutron Source, a DOE Office of Science User Facility operated by the Oak Ridge National Laboratory, on proposal number IPTS-34379. Use of the MAD beamline at the McMaster Nuclear Reactor for crystal alignment is supported by McMaster University and the Canada Foundation for Innovation.

[1] L. D. C. Jaubert, Topology of the vacuum, in *Spin Ice*, edited by M. Udagawa and L. Jaubert (Springer Interna-

tional Publishing, Cham, 2021) pp. 117–141.

[2] T. Fennell, O. A. Petrenko, B. Fåk, S. T. Bramwell, M. Enjalran, T. Yavors'kii, M. J. P. Gingras, R. G. Melko, and G. Balakrishnan, Neutron scattering investigation of the spin ice state in  $\text{Dy}_2\text{Ti}_2\text{O}_7$ , *Phys. Rev. B* **70**, 134408 (2004).

[3] D. J. P. Morris, D. A. Tennant, S. A. Grigera, B. Klemke, C. Castelnovo, R. Moessner, C. Czternasty, M. Meissner, K. C. Rule, J.-U. Hoffmann, K. Kiefer, S. Gerischer, D. Slobinsky, and R. S. Perry, Dirac Strings and Magnetic Monopoles in the Spin Ice  $\text{Dy}_2\text{Ti}_2\text{O}_7$ , *Science* **326**, 411 (2009).

[4] T. Fennell, P. P. Deen, A. R. Wildes, K. Schmalzl, D. Prabhakaran, A. T. Boothroyd, R. J. Aldus, D. F. McMorrow, and S. T. Bramwell, Magnetic Coulomb Phase in the Spin Ice  $\text{Ho}_2\text{Ti}_2\text{O}_7$ , *Science* **326**, 415 (2009).

[5] J. P. Clancy, J. P. C. Ruff, S. R. Dunsiger, Y. Zhao, H. A. Dabkowska, J. S. Gardner, Y. Qiu, J. R. D. Copley, T. Jenkins, and B. D. Gaulin, Revisiting static and dynamic spin-ice correlations in  $\text{Ho}_2\text{Ti}_2\text{O}_7$  with neutron scattering, *Phys. Rev. B* **79**, 014408 (2009).

[6] T. Yavors'kii, T. Fennell, M. J. P. Gingras, and S. T. Bramwell,  $\text{Dy}_2\text{Ti}_2\text{O}_7$  Spin Ice: A Test Case for Emergent Clusters in a Frustrated Magnet, *Phys. Rev. Lett.* **101**, 037204 (2008).

[7] P. Henelius, T. Lin, M. Enjalran, Z. Hao, J. G. Rau, J. Altona, F. Flicker, T. Yavors'kii, and M. J. P. Gingras, Refrstration and competing orders in the prototypical  $\text{Dy}_2\text{Ti}_2\text{O}_7$  spin ice material, *Phys. Rev. B* **93**, 024402 (2016).

[8] M. Hermele, M. P. A. Fisher, and L. Balents, Pyrochlore photons: The  $U(1)$  spin liquid in a  $S = \frac{1}{2}$  three-dimensional frustrated magnet, *Phys. Rev. B* **69**, 064404 (2004).

[9] M. J. P. Gingras and P. A. McClarty, Quantum spin ice: a search for gapless quantum spin liquids in pyrochlore magnets, *Reports on Progress in Physics* **77**, 056501 (2014).

[10] O. Benton, O. Sikora, and N. Shannon, Seeing the light: Experimental signatures of emergent electromagnetism in a quantum spin ice, *Phys. Rev. B* **86**, 075154 (2012).

[11] K. A. Ross, L. Savary, B. D. Gaulin, and L. Balents, Quantum Excitations in Quantum Spin Ice, *Phys. Rev. X* **1**, 021002 (2011).

[12] A. M. Hallas, J. Gaudet, M. N. Wilson, T. J. Munsie, A. A. Aczel, M. B. Stone, R. S. Freitas, A. M. Arevalo-Lopez, J. P. Attfield, M. Tachibana, C. R. Wiebe, G. M. Luke, and B. D. Gaulin, XY antiferromagnetic ground state in the effective  $S = \frac{1}{2}$  pyrochlore  $\text{Yb}_2\text{Ge}_2\text{O}_7$ , *Phys. Rev. B* **93**, 104405 (2016).

[13] A. Scheie, J. Kindervater, S. Zhang, H. J. Changlani, G. Sala, G. Ehlers, A. Heinemann, G. S. Tucker, S. M. Koohpayeh, and C. Broholm, Multiphase magnetism in  $\text{Yb}_2\text{Ti}_2\text{O}_7$ , *Proceedings of the National Academy of Sciences* **117**, 27245 (2020).

[14] M. Powell, L. D. Sanjeewa, C. D. McMillen, K. A. Ross, C. L. Sarkis, and J. W. Kolis, Hydrothermal Crystal Growth of Rare Earth Tin Cubic Pyrochlores,  $\text{RE}_2\text{Sn}_2\text{O}_7$  ( $\text{RE} = \text{La-Lu}$ ): Site Ordered, Low Defect Single Crystals, *Crystal Growth & Design* **19**, 4920 (2019).

[15] J. P. C. Ruff, J. P. Clancy, A. Bourque, M. A. White, M. Ramazanoglu, J. S. Gardner, Y. Qiu, J. R. D. Copley, M. B. Johnson, H. A. Dabkowska, and B. D. Gaulin, Spin Waves and Quantum Criticality in the Frustrated XY Pyrochlore Antiferromagnet  $\text{Er}_2\text{Ti}_2\text{O}_7$ , *Phys. Rev. Lett.* **101**, 147205 (2008).

[16] L. Savary, K. A. Ross, B. D. Gaulin, J. P. C. Ruff, and L. Balents, Order by Quantum Disorder in  $\text{Er}_2\text{Ti}_2\text{O}_7$ , *Phys. Rev. Lett.* **109**, 167201 (2012).

[17] D. R. Yahne, D. Pereira, L. D. C. Jaubert, L. D. Sanjeewa, M. Powell, J. W. Kolis, G. Xu, M. Enjalran, M. J. P. Gingras, and K. A. Ross, Understanding Reentrance in Frustrated Magnets: The Case of the  $\text{Er}_2\text{Sn}_2\text{O}_7$  Pyrochlore, *Phys. Rev. Lett.* **127**, 277206 (2021).

[18] K. Kimura, S. Nakatsuji, J.-J. Wen, C. Broholm, M. B. Stone, E. Nishibori, and H. Sawa, Quantum fluctuations in spin-ice-like  $\text{Pr}_2\text{Zr}_2\text{O}_7$ , *Nature Communications* **4**, 1934 (2013).

[19] N. Martin, P. Bonville, E. Lhotel, S. Guitteny, A. Wildes, C. Decorse, M. Ciomaga Hatnean, G. Balakrishnan, I. Mirebeau, and S. Petit, Disorder and Quantum Spin Ice, *Phys. Rev. X* **7**, 041028 (2017).

[20] J.-J. Wen, S. M. Koohpayeh, K. A. Ross, B. A. Trump, T. M. McQueen, K. Kimura, S. Nakatsuji, Y. Qiu, D. M. Pajerowski, J. R. D. Copley, and C. L. Broholm, Disordered Route to the Coulomb Quantum Spin Liquid: Random Transverse Fields on Spin Ice in  $\text{Pr}_2\text{Zr}_2\text{O}_7$ , *Phys. Rev. Lett.* **118**, 107206 (2017).

[21] T. J. Hicken, P. Meadows, D. Prabhakaran, A. Szabó, S. E. Dutton, C. Castelnovo, K. Moovendaran, T. S. N. de la Fuente, L. Mangin-Thro, G. B. G. Stenning, M. J. Gutmann, G. Sala, M. B. Stone, P. F. Henry, D. J. Voneshen, and J. P. Goff, Intrinsic disorder in the candidate quantum spin ice  $\text{Pr}_2\text{Zr}_2\text{O}_7$  (2025), arXiv:2509.10101 [cond-mat.str-el].

[22] Y. Luo, J. A. M. Paddison, B. R. Ortiz, M. Knudsson, S. D. Wilson, J. Liu, B. A. Frandsen, S. A. Chen, M. Frontzek, A. Podlesnyak, and A. A. Aczel, Disorder-induced proximate quantum spin ice phase in  $\text{Pr}_2\text{Sn}_2\text{O}_7$  (2025), arXiv:2508.19248 [cond-mat.str-el].

[23] Y.-P. Huang, G. Chen, and M. Hermele, Quantum Spin Ices and Topological Phases from Dipolar-Octupolar Doublets on the Pyrochlore Lattice, *Phys. Rev. Lett.* **112**, 167203 (2014).

[24] E. M. Smith, E. Lhotel, S. Petit, and B. D. Gaulin, Experimental insights into quantum spin ice physics in dipole-octupole pyrochlore magnets, *Annual Review of Condensed Matter Physics* **16**, 387 (2025).

[25] F. Desrochers and Y. B. Kim, Spectroscopic Signatures of Fractionalization in Octupolar Quantum Spin Ice, *Phys. Rev. Lett.* **132**, 066502 (2024).

[26] O. Benton, Ground-state phase diagram of dipolar-octupolar pyrochlores, *Phys. Rev. B* **102**, 104408 (2020).

[27] S. Petit, E. Lhotel, B. Canals, M. Ciomaga Hatnean, J. Ollivier, H. Mutka, E. Ressouche, A. . R. Wildes, M. R. Lees, and G. Balakrishnan, Observation of magnetic fragmentation in spin ice, *Nature Physics* **12**, 746 (2016).

[28] O. Benton, Quantum origins of moment fragmentation in  $\text{Nd}_2\text{Zr}_2\text{O}_7$ , *Phys. Rev. B* **94**, 104430 (2016).

[29] J. Xu, O. Benton, V. K. Anand, A. T. M. N. Islam, T. Guidi, G. Ehlers, E. Feng, Y. Su, A. Sakai, P. Gegenwart, and B. Lake, Anisotropic exchange Hamiltonian, magnetic phase diagram, and domain inversion of  $\text{Nd}_2\text{Zr}_2\text{O}_7$ , *Phys. Rev. B* **99**, 144420 (2019).

[30] Y. Luo, M. Powell, J. A. M. Paddison, B. R. Ortiz, J. R. Stewart, J. W. Kolis, and A. A. Aczel, Magnetic Moment Fragmentation in an All-in-All-out Pyrochlore  $\text{Nd}_2\text{Sn}_2\text{O}_7$  (2025), arXiv:2510.04845 [cond-mat.str-el].

[31] R. Sibille, E. Lhotel, V. Pomjakushin, C. Baines, T. Fennell, and M. Kenzelmann, Candidate Quantum Spin Liquid in the Ce<sup>3+</sup> Pyrochlore Stannate Ce<sub>2</sub>Sn<sub>2</sub>O<sub>7</sub>, *Phys. Rev. Lett.* **115**, 097202 (2015).

[32] J. Gaudet, E. M. Smith, J. Dudemaine, J. Beare, C. R. C. Buhariwalla, N. P. Butch, M. B. Stone, A. I. Kolesnikov, G. Xu, D. R. Yahne, K. A. Ross, C. A. Marjerrison, J. D. Garrett, G. M. Luke, A. D. Bianchi, and B. D. Gaulin, Quantum Spin Ice Dynamics in the Dipole-Octupole Pyrochlore Magnet Ce<sub>2</sub>Zr<sub>2</sub>O<sub>7</sub>, *Phys. Rev. Lett.* **122**, 187201 (2019).

[33] B. Gao, T. Chen, D. W. Tam, C.-L. Huang, K. Sasmal, D. T. Adroja, F. Ye, H. Cao, G. Sala, M. B. Stone, C. Baines, J. A. T. Verezhak, H. Hu, J.-H. Chung, X. Xu, S.-W. Cheong, M. Nallaiyan, S. Spagna, M. B. Maple, A. H. Nevidomskyy, E. Morosan, G. Chen, and P. Dai, Experimental signatures of a three-dimensional quantum spin liquid in effective spin-1/2 Ce<sub>2</sub>Zr<sub>2</sub>O<sub>7</sub> pyrochlore, *Nature Physics* **15**, 1052 (2019).

[34] R. Sibille, N. Gauthier, E. Lhotel, V. Porée, V. Pomjakushin, R. A. Ewings, T. G. Perring, J. Ollivier, A. Wildes, C. Ritter, T. C. Hansen, D. A. Keen, G. J. Nilsen, L. Keller, S. Petit, and T. Fennell, A quantum liquid of magnetic octupoles on the pyrochlore lattice, *Nature Physics* **16**, 546 (2020).

[35] E. M. Smith, O. Benton, D. R. Yahne, B. Placke, R. Schäfer, J. Gaudet, J. Dudemaine, A. Fitterman, J. Beare, A. R. Wildes, S. Bhattacharya, T. DeLazzer, C. R. C. Buhariwalla, N. P. Butch, R. Movshovich, J. D. Garrett, C. A. Marjerrison, J. P. Clancy, E. Kermarrec, G. M. Luke, A. D. Bianchi, K. A. Ross, and B. D. Gaulin, Case for a U(1)<sub>π</sub> Quantum Spin Liquid Ground State in the Dipole-Octupole Pyrochlore Ce<sub>2</sub>Zr<sub>2</sub>O<sub>7</sub>, *Phys. Rev. X* **12**, 021015 (2022).

[36] E. M. Smith, J. Dudemaine, B. Placke, R. Schäfer, D. R. Yahne, T. DeLazzer, A. Fitterman, J. Beare, J. Gaudet, C. R. C. Buhariwalla, A. Podlesnyak, G. Xu, J. P. Clancy, R. Movshovich, G. M. Luke, K. A. Ross, R. Moessner, O. Benton, A. D. Bianchi, and B. D. Gaulin, Quantum spin ice response to a magnetic field in the dipole-octupole pyrochlore Ce<sub>2</sub>Zr<sub>2</sub>O<sub>7</sub>, *Phys. Rev. B* **108**, 054438 (2023).

[37] J. Beare, E. M. Smith, J. Dudemaine, R. Schäfer, M. R. Rutherford, S. Sharma, A. Fitterman, C. A. Marjerrison, T. J. Williams, A. A. Aczel, S. R. Dunsiger, A. D. Bianchi, B. D. Gaulin, and G. M. Luke, μSR study of the dipole-octupole quantum spin ice candidate Ce<sub>2</sub>Zr<sub>2</sub>O<sub>7</sub>, *Phys. Rev. B* **108**, 174411 (2023).

[38] D. R. Yahne, B. Placke, R. Schäfer, O. Benton, R. Moessner, M. Powell, J. W. Kolis, C. M. Pasco, A. F. May, M. D. Frontzek, E. M. Smith, B. D. Gaulin, S. Calder, and K. A. Ross, Dipolar Spin Ice Regime Proximate to an All-In-All-Out Néel Ground State in the Dipolar-Octupolar Pyrochlore Ce<sub>2</sub>Sn<sub>2</sub>O<sub>7</sub>, *Phys. Rev. X* **14**, 011005 (2024).

[39] V. Porée, A. Bhardwaj, E. Lhotel, S. Petit, N. Gauthier, H. Yan, V. Pomjakushin, J. Ollivier, J. A. Quilliam, A. H. Nevidomskyy, H. J. Changlani, and R. Sibille, Dipolar-octupolar correlations and hierarchy of exchange interactions in Ce<sub>2</sub>Hf<sub>2</sub>O<sub>7</sub>, *Phys. Rev. B* **112**, L180404 (2025).

[40] E. M. Smith, A. Fitterman, R. Schäfer, B. Placke, A. Woods, S. Lee, S. H.-Y. Huang, J. Beare, S. Sharma, D. Chatterjee, C. Balz, M. B. Stone, A. I. Kolesnikov, A. R. Wildes, E. Kermarrec, G. M. Luke, O. Benton, R. Moessner, R. Movshovich, A. D. Bianchi, and B. D. Gaulin, Two-Peak Heat Capacity Accounts for Rln(2) Entropy and Ground State Access in the Dipole-Octupole Pyrochlore Ce<sub>2</sub>Hf<sub>2</sub>O<sub>7</sub>, *Phys. Rev. Lett.* **135**, 086702 (2025).

[41] E. M. Smith, R. Schäfer, J. Dudemaine, B. Placke, B. Yuan, Z. Morgan, F. Ye, R. Moessner, O. Benton, A. D. Bianchi, and B. D. Gaulin, Single-Crystal Diffuse Neutron Scattering Study of the Dipole-Octupole Quantum Spin-Ice Candidate Ce<sub>2</sub>Zr<sub>2</sub>O<sub>7</sub>: No Apparent Octupolar Correlations Above  $T = 0.05$  K, *Phys. Rev. X* **15**, 021033 (2025).

[42] V. Porée, H. Yan, F. Desrochers, S. Petit, E. Lhotel, M. Appel, J. Ollivier, Y. B. Kim, A. H. Nevidomskyy, and R. Sibille, Evidence for fractional matter coupled to an emergent gauge field in a quantum spin ice, *Nature Physics* **21**, 83 (2025).

[43] B. Gao, F. Desrochers, D. W. Tam, D. M. Kirschbaum, P. Steffens, A. Hiess, D. H. Nguyen, Y. Su, S.-W. Cheong, S. Paschen, Y. B. Kim, and P. Dai, Neutron scattering and thermodynamic evidence for emergent photons and fractionalization in a pyrochlore spin ice, *Nature Physics* **21**, 1203 (2025).

[44] E. Kermarrec, G. Chen, H. Okamoto, C.-J. Huang, H. Yan, J. Yan, H. Takeda, Y. Shimizu, E. M. Smith, A. Fitterman, A. D. Bianchi, B. D. Gaulin, and M. Yamashita, Magnetization and magnetostriction measurements of the dipole-octupole quantum spin ice candidate ce2hf2o7 (2025), arXiv:2509.09189 [cond-mat.str-el].

[45] A. Bhardwaj, S. Zhang, H. Yan, R. Moessner, A. H. Nevidomskyy, and H. J. Changlani, Sleuthing out exotic quantum spin liquidity in the pyrochlore magnet Ce<sub>2</sub>Zr<sub>2</sub>O<sub>7</sub>, *npj Quantum Materials* **7**, 51 (2022).

[46] F. Ye, Y. Liu, R. Whitfield, R. Osborn, and S. Rosenkranz, Implementation of cross correlation for energy discrimination on the time-of-flight spectrometer CORELLI, *Journal of Applied Crystallography* **51**, 315 (2018).

[47] J. Xu, O. Benton, A. T. M. N. Islam, T. Guidi, G. Ehlers, and B. Lake, Order out of a Coulomb Phase and Higgs Transition: Frustrated Transverse Interactions of Nd<sub>2</sub>Zr<sub>2</sub>O<sub>7</sub>, *Phys. Rev. Lett.* **124**, 097203 (2020).

[48] See Fig. S12 (a) of Ref. [40] for NLC calculations using a parameter set very similar to that proposed for Ce<sub>2</sub>Sn<sub>2</sub>O<sub>7</sub>.

[49] J. G. Rau and M. J. P. Gingras, Magnitude of quantum effects in classical spin ices, *Phys. Rev. B* **92**, 144417 (2015).